P33 LIDAR OBSERVATIONS OF FINE-SCALE ATMOSPHERIC GRAVITY WAVES IN THE NOCTURNAL BOUNDARY LAYER ABOVE AN ORCHARD CANOPY

Tyson N. Randall, Elizabeth R. Jachens, Shane D. Mayor*

California State University, Chico

ABSTRACT

Fifty-two episodes of micrometeorological gravity wave activity were identified in data collected with the Raman-shifted Eye-safe Aerosol Lidar (REAL) near Dixon, California, during a nearly continuous 3-month period of observation. The internal waves, with wavelengths ranging from 40 m to 100 m, appear in horizontal cross-sectional elastic backscatter images of the atmospheric roughness sublayer between 10 m and 30 m AGL. All of the episodes occur at night when the atmosphere tends toward stability. Time-series data from in situ sensors mounted to a tower that intersected the lidar scans at 1.6 km range reveal oscillations in all three wind-velocity components and in some cases the temperature and relative humidity traces. We hypothesize that the lidar can reveal these waves because of the existence of vertical gradients of aerosol backscatter and the oscillating vertical component of air motion in the wave train that displace the backscatter gradients vertically.

1. INTRODUCTION

The atmospheric boundary layer (ABL) is the part of the troposphere that is directly influenced by the presence of the earth's surface, and responds to surface forcings with a timescale of about an hour or less (Stull, 1988). During the daytime and over land, the ABL is usually hundreds of meters to a kilometer or more in depth and is characterized by large eddies that mix heat, moisture, trace gases, pollutants, and momentum very effectively in both the horizontal and vertical dimensions. At night, radiant energy from the sun is no longer available to warm the surface and drive convective thermals. As a result, the nocturnal ABL tends toward static stability supporting stratification, vertical wind shear, gravity wave activity, and intermittent turbulence confined to shallow layers.

This complex nocturnal flow regime presents significant observational and modeling challenges. In this paper, we report on new atmospheric lidar observations of what appear to be fine-scale waves within 20 m of the top of an orchard canopy. Observations in the form of time-series and limited amounts of spatial sampling from previous studies have revealed wave-like oscillations at night in this shallow region above forest canopies (Bergström and Högström, 1989; Cava et al., 2004; Fitzjarrald and Moore, 1990; Kaimal and Finnigan, 1994; Lee, 1997; Lee et al., 1997; Lee and Barr, 1998; Van Gorsel et al., 2011). However, we could not find any papers on lidar observations of canopy waves. This may be due to the difficulty of observing the waves in the very shallow layer immediately above treetops. Herein we report on our preliminary investigations of what appear to be canopy waves observed with the Raman-shifted Eye-safe Aerosol Lidar (REAL) (Mayor et al., 2007) during the 2007 Canopy Horizontal Array Turbulence Study (CHATS) (Patton et al., 2011). The REAL is a ground-based elastic backscatter lidar operating at an eye-safe wavelength of 1.54 microns.

*Corresponding author address: Shane D. Mayor, Department of Physics, California State University, Chico, Chico, CA, 95929; e-mail: sdmayor@csuchico.edu

2. EXPERIMENTAL SETUP

CHATS took place in Dixon, California, from 15 March through 11 June 2007. The REAL was located 1.61 km directly north of a 30 m tall vertical tower (Figure 1) equipped with thirteen three-component sonic anemometers, temperature, and relative humidity sensors (Figure 2). The lidar scanned at a sufficiently low elevation angle as to intersect the vertical tower at about 18-20 m AGL. Wide scans covered 60 degrees of azimuth and narrow scans 10 degrees of azimuth. The update rate for scan images depended on the azimuthal range and scan rate and ranged between 10 s and 40 s per scan.

Figure 1: Plan view of the experimental area for the 2007 CHATS experiment. The REAL was located 1.61 km directly north of the 30-m tall NCAR ISFF tower. We limited our analysis to the 1 km^2 box centered on the tower.

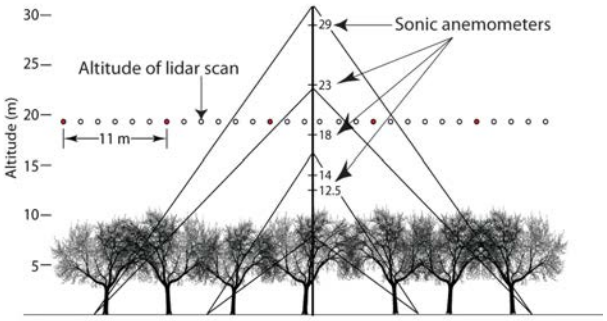

Figure 2: Arrangement of wind, temperature, and humidity sensors above the trees on the NCAR ISFF 30-m tower. Sensors below the canopy top not shown.

3. HYPOTHESIS

The first question that we wish to address is "Why is the REAL capable of detecting canopy waves?" We hypothesize that during the evening and night, as the earth's surface cools and the atmospheric surface layer tends toward stability, the lower atmosphere becomes stratified with layers that are horizontally homogeneous in terms of temperature, relative humidity, and aerosol concentration.

However, the variation in these properties may change significantly with height (Figure 3). These aerosol strata may then be displaced vertically by internal gravity waves (Figure 4). The horizontally scanning lidar beam may then penetrate and reveal the waves as shown in Figure 5.

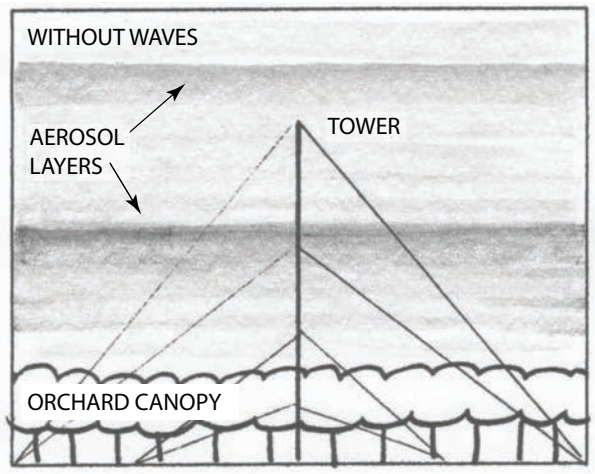

Figure 3: Sketch of a vertical cross-section of the lower atmosphere (from the surface to about 40 m AGL) that may occur at night during quiescent conditions. Stable stratification and weak flow result in the formation of vertical gradients of aerosol backscatter that are horizontally invariant.

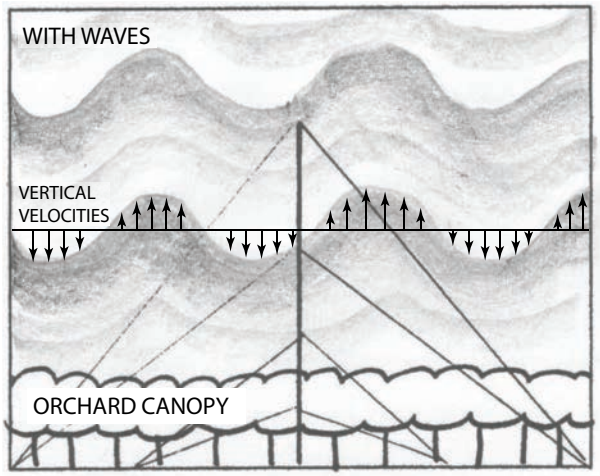

Figure 4: Sketch of a vertical cross-section of the lower atmosphere showing how the vertical wind component, w, caused by internal gravity waves can vertically displace the horizontal aerosol strata shown in Figure 4 and enable the elastic backscatter lidar to observe the wave structure in a near-horizontal plane. The horizontal line above is the approximate altitude of the horizontal lidar scans.

4. OBSERVATIONS

Time-lapse animations of more than 1800 hours of high-pass filtered REAL images from the entire CHATS data set were created*. The animations of nearly horizontal scans were carefully examined for the presence of fine-scale wave packets. A wave packet is distinct from other flow features observed in the lidar images in that the linear bands of enhanced backscatter intensity tend to be oriented perpendicular to the wind direction and the direction in which they propagate. Furthermore, they appear to have a high degree of spatial and temporal coherence compared to plumes and wind parallel streaks sometimes observed during periods of turbulent flow. For a wave packet to be included in this study, it must have passed through the tower (located 1.6 km directly south of the lidar) and have a lifetime longer than one minute. Our subjective judgments of the coherence of the wave packets were based on the clear identification of crests and troughs and movement together as a group. Fifty-two wave episodes met the criteria.

5. DISCUSSION

All fifty-two episodes occurred between 5:00 and 14:00 UTC (22:00 and 7:00 PDT) during stable nighttime conditions. The average wave episode duration was about 12 min while episodes ranged from 1 min 43 s to 1 hr 10 min 37 s. Wave episodes were detected on 28 of the 86 nights of CHATS. All figures in this paper are from 14 May 2007.

*Time-lapse animations are available for viewing at http://www.phys.csuchico.edu/lidar

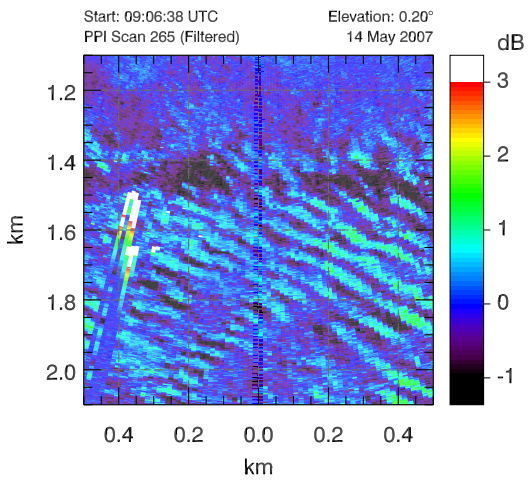

Figure 5: 1 km^2 horizontal scan from 14 May 2007, revealing waves in the high-pass median filtered backscatter signal and therefore the vertical velocities. Such images can be used to determine wavelength subjectively. In this case, wavelength is approximately 60 m.

5.1. Temporal Data

After the wave episodes were identified in the lidar data, the corresponding temporal data from the tower was studied. Vertically coherent oscillations in the vertical velocity (Figure 6) confirm our hypothesis that the perturbations in the backscatter are related to perturbations in vertical velocities and have a dynamic cause. Through subjective inspection, periods were determined to be between 20 s and 2 min. Tower data also reveal oscillations, speed shear, and directional shear in the horizontal velocities (Figure 7).

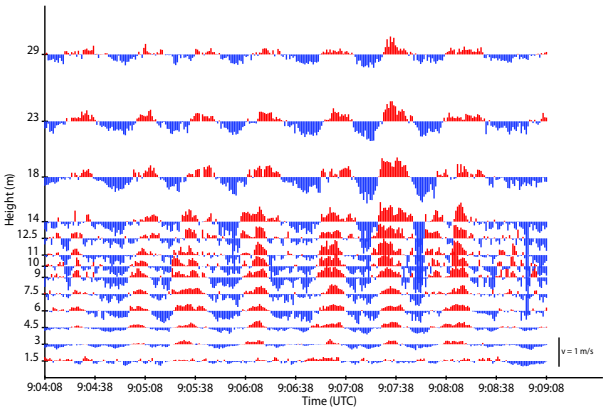

Figure 6: 5 min time-series of vertical velocity from the wave episode on 14 May 2007. Upward motions are in red and downward are in blue. Oscillations are vertically coherent to from inside the canopy (<10 m) to the top of the tower (29 m).

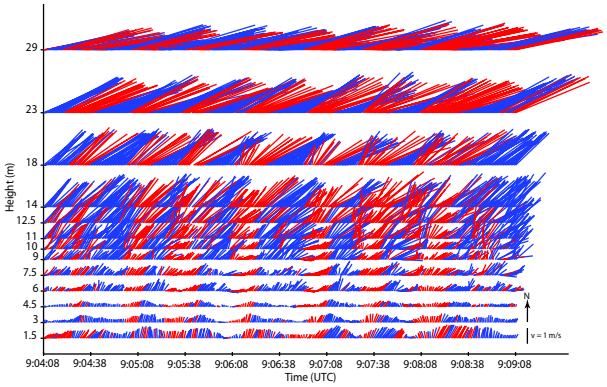

Figure 7: The same 5 min interval for the horizontal velocities. Upward motions are in red and downward are in blue. Horizontal velocities reveal oscillations, speed shear and directional shear through the top of the tower.

Temperature profiles during these episodes all show stable conditions (Figure 8). From these values, we calculated Brunt–Väisälä frequencies, N, from the equation

$$N = \sqrt{\frac{g}{\theta}\frac{d\theta}{dz}} \tag{1}$$

where g is acceleration due to gravity, θ is the potential temperature, and z is the height above ground level. Using the near-surface approximation:

$$T \approx \theta \tag{2}$$

where T is temperature, we can obtain a theoretical period, P:

$$P = \frac{2\pi}{N} \tag{3}$$

Theoretical periods range from 45 s to several minutes agree with our observations to within an order of magnitude but show no correlation.

Figure 9 shows a time-series of temperature and vertical velocity perturbations. A 90-degree phase shift is apparent, which is expected to result in a low thermal flux. We confirmed this by calculating the covariance of these time-series. This phase shift also appears between the vertical and horizontal velocities. We have also confirmed that momentum fluxes are near zero.

5.2. Spatial Data

The REAL has the unique capability to observe spatial characteristics of these waves. Wavelength was measured subjectively for all the cases and ranged between 40 and 100 m. For the 22 cases with a sufficiently short time between frames ($\leq$17 s between scans) a propagation direction and phase speed was also determined by

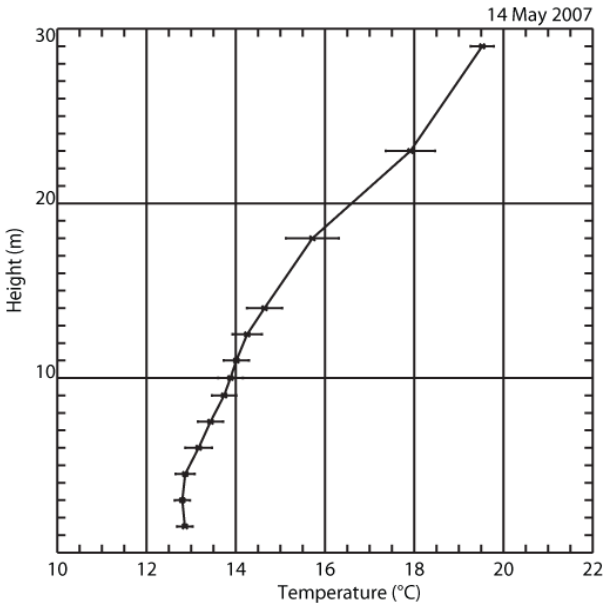

Figure 8: Temperature profile during a wave episode. This shows the average temperature at each height on the tower during the 14 May episode, and the horizontal bars show the standard deviation during the wave episode.

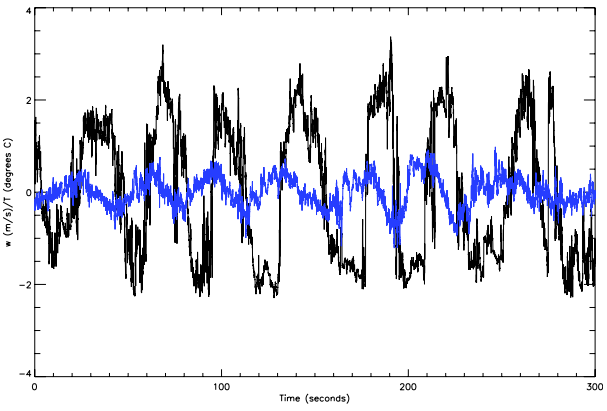

Figure 9: Vertical velocity (blue) and temperature (black) perturbation as a function of time. A 90 degree phase shift is apparent, leading to a near zero thermal flux.

looking at the displacement of a wave front in consecutive scans. The propagation direction is in the direction of the mean flow (Figure 10) while the phase speed tends to be slower than the wind by roughly a factor of two (not shown).

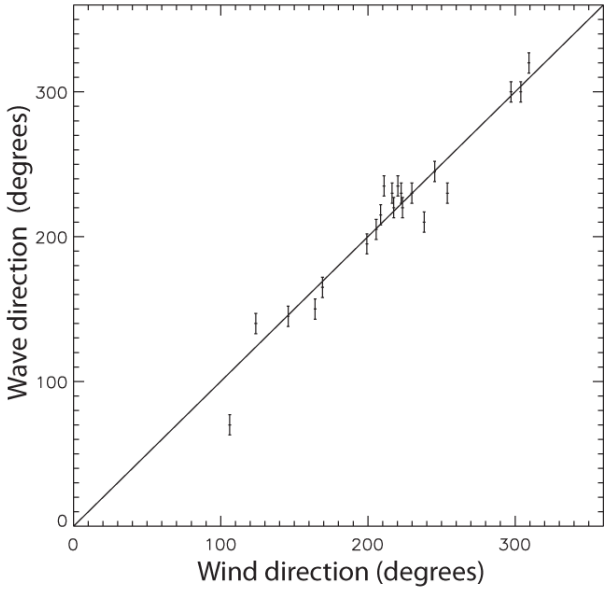

Figure 10: Plot of wave propagation direction (determined subjectively) versus wind direction at 18 m from the sonic anemometer for 22 wave cases showing that the waves are propagating in the direction of the mean flow.

In order to make an objective measure of the wavelength, we computed autocorrelation functions for 12 of the cases with strong backscatter intensity without large spikes. We mapped the lidar backscatter data, $\beta(r, \theta, t)$ from its native polar coordinates to a Cartesian grid, $\beta(x, y, t)$. Then, following our previous conclusion that these waves propagate in the direction of the wind, we rotated the Cartesian coordinate system so that the x-direction was in the direction of the mean flow at 18 m. We then computed the autocorrelation function, R, for a space series at the position y_0 at time t_0 (Figure 11).

$$R = F^{-1}[F[\beta(x, y_0, t_0)] * conj(F[\beta(x, y_0, t_0)])] \quad (4)$$

where F is the fast Fourier transform. We determined the wavelength was associated with the first local maximum of R (Figure 12). This analysis lead to values for wavelength consistent with each of our subjective measurements, ranging from 41 to 112 m.

6. CONCLUSION

The horizontally scanning eye-safe elastic backscatter lidar can identify and confirm the presence of fine-scale gravity waves over forest canopies. The lidar images

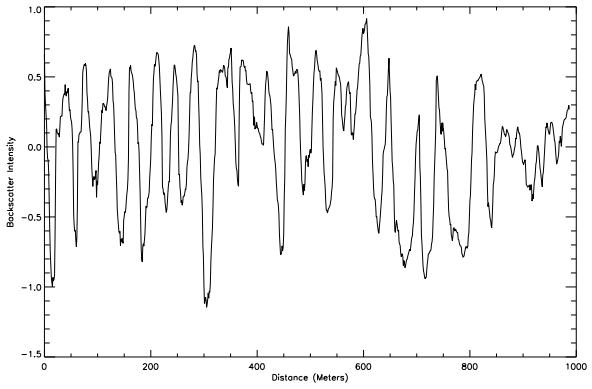

Figure 11: Horizontal slice of range-corrected, high–pass median filtered backscatter intensity from 14 May 2007 at 9:06:38 UTC in the streamwise coordinate system.

contain quantitative spatial information such as wavelength that is not available from in situ time-series data. With a sufficient scan-rate, wave propagation direction and phase speed can also be determined. A key requirement for such lidar measurements is high spatial resolution images and sensitivity to small changes in aerosol backscatter. Radial high-pass median filtering is used to clarify the presence of the waves in the images. We note the spacing of backscatter data points in the radial direction of the REAL data is 1.5 m. This enables the instrument to resolve these wave structures that occur on scales of tens of meters. Preliminary analyses show that these waves transport little to no heat or momentum and all of the episodes occur during statically stable conditions.

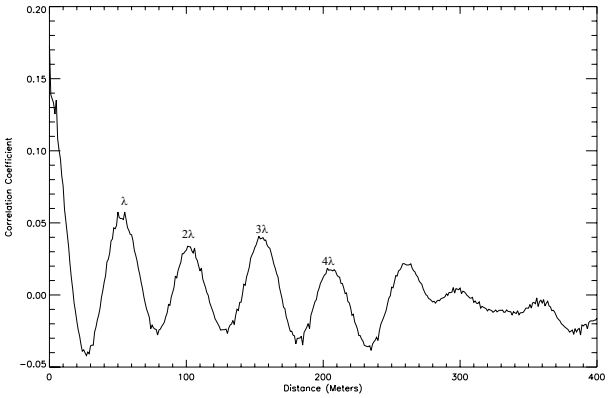

Figure 12: Autocorrelation function for slice in Figure 11 shows peaks at wavelength-multiples, the first of which is at 55 m agreeing the subjective measurement 60 m.

7. ACKNOWLEDGMENTS

This study was conducted with support from the National Science Foundation, under Grant 0924407.

REFERENCES

Bergström, H. and U. Högström, 1989: Turbulent exchange above a pine forest. 2. organized structures, *Bound. Layer Meteor.*, **49**, 231–263.

Cava, D., U. Giostra, M. Siqueira, and G. Katul, 2004: Organised motion and radiative perturbations in the nocturnal canopy sublayer above an even-aged pine forest, *Bound. Layer Meteor.*, **112**, 129–157.

Fitzjarrald, D. R. and K. E. Moore, 1990: Mechanisms of nocturnal exchange between the rain forest and the atmosphere, *J. Geophys. Res*, **95(D10)**, 16,839–16,850.

Kaimal, J. C. and J. J. Finnigan, 1994: *Atmospheric Boundary Layer Flows*, Oxford University Press, 200 Madison Ave., New York, NY 10016, 289 pp.

Lee, X., 1997: Gravity waves in a forest: A linear analysis, *J. Atmos. Sci.*, **54**, 2574–2585.

Lee, X. and A. G. Barr, 1998: Climatology of gravity waves in a forest, *Quart. J. R. Met. Soc.*, **124**, 1403–1419.

Lee, X., H. H. Neumann, G. D. Hartog, J. D. Fuentes, T. A. Black, R. E. Mickle, P. C. Yang, and P. D. Blanken, 1997: Observation of gravity waves in a boreal forest, *Bound. Layer Meteor.*, **84**, 383–398.

Mayor, S. D., S. M. Spuler, B. M. Morley, and E. Loew, 2007: Polarization lidar at 1.54-microns and observations of plumes from aerosol generators, *Opt. Eng.*, **46**, DOI: 10.1117/12.781902.

Patton, E. G., T. W. Horst, P. P. Sullivan, D. H. Lenschow, S. P. Oncley, W. O. J. Brown, S. P. Burns, A. B. Guenther, A. Held, T. Karl, S. D. Mayor, L. V. Rizzo, S. M. Spuler, J. Sun, A. A. Turnipseed, E. J. Allwine, S. L. Edburg, B. K. Lamb, R. Avissar, R. Calhoun, J. Kleissl, W. J. Massman, K. T. P. U, and J. C. Weil, 2011: The Canopy Horizontal Array Turbulence Study (CHATS), *Bull. Amer. Meteor. Soc.*, **92**, 593–611.

Stull, R. B., 1988: *An Introduction to Boundary Layer Meteorology*, Kluwer, Boston.

Van Gorsel, E., I. N. Harman, J. J. Finnigan, and R. Leuning, 2011: Decoupling of air flow above and in plant canopies and gravity waves affect micrometeorological estimates of net scalar exchange, *Agr. Forest Meteorol.*, **151**, 927–933.